Nonlocal Multiscale Single Image Statistics From Sentinel-1 SAR Data for High Resolution Bitemporal Forest Wind Damage Detection

Manninen, T.

2022

Manninen , T , Jaaskelainen , E & Tomppo , E 2022 , ' Nonlocal Multiscale Single Image Statistics From Sentinel-1 SAR Data for High Resolution Bitemporal Forest Wind Damage Detection ' , IEEE Geoscience and Remote Sensing Letters , vol. 19 , 2504705 . https://doi.org/10.1109/LGRS.2022.

http://hdl.handle.net/10138/353676
https://doi.org/10.1109/LGRS.2022.3169473

unspecified
acceptedVersion

Non-local multi-scale single image statistics from Sentinel-1 SAR data for high resolution bitemporal forest wind damage detection

T. Manninen, E. Jääskeläinen and E. Tomppo

***Abstract*— Change detection of Synthetic Aperture Radar (SAR) data is a challenge for high resolution applications. This study presents a new non-local averaging approach (STATSAR) to reduce the speckle of single Sentinel-1 SAR images and statistical parameters derived from the image. The similarity of SAR pixels is based on the statistics of 3 x 3 window as represented by the mean, standard deviation, median, minimum, and maximum. K-means clustering is used to divide the SAR image in 30 similarity clusters. The non-local averaging is carried out within each cluster separately in magnitude order of the 3x3 window averages. The non-local filtering is applicable not only to the original pixel backscattering values, but also to statistical parameters, such as standard deviation. The statistical parameters to be filtered can represent any window size, according to the need of the application.**

The non-locally averaged standard deviation derived in two spatial resolutions, 3 x 3 and 7 x 7 windows, are demonstrated here for improving the resolution in which the forest damages can be detected using the VH polarized backscattering spatial variation change.

***Index Terms*— SAR Data, Vegetation and Land Surface.**

I. Introduction

CHANGE detection using Synthetic Aperture Radar (SAR) images has been actively studied since the availability of SAR images. The launch of the Sentinel-1 (S1) satellites provides a possibility to observe abrupt changes, especially in northern latitudes, where the coverage of the open access imagery is almost daily.

The main strategy of change detection has consisted of 1) preprocessing, 2) taking the difference and 3) post-processing [1] of the backscattered intensity. The important step has been the denoising of the images to be compared. High-resolution SAR image analysis is typically based on non-local mean filtering, if multitemporal averaging is not possible [2][3][4][5][6][7][8][9][10][11][12][13]. Recently also deep learning algorithms have been developed for change detection [14][15].

When the change detection information is not needed quickly, it is possible to use multitemporal image analysis to observe the changes. However, in many cases, such as forest damages, the information is needed as soon as possible. Then it is desirable to use a change detection method that can handle images bitemporally. In this study we demonstrate detection of forest damages using S1 data, but instead of despeckling the backscattered intensity, its statistical parameters are non-locally filtered to reduce the speckle.

C-band is challenging in observing changes in forests, due to the small wavelength that is to a large extent attenuated by the forest. In a recent study [16][17] it was noticed that the stand level standard deviation of the VH polarized backscattering changes when the forest is damaged. If all trees of a stand are fallen due to strong wind, the mean VH standard deviation of the stand is markedly smaller than before the storm.

However, forest damages caused by winds do not follow the boundaries of the management units, such as stands. The storm areas vary by size, from smaller than one hectare to several hundreds or thousands of hectares. Thus, a method sensitive to small areas, such as a group of pixels would also be needed.

Detection of forest damage in high resolution consists of two problems: 1) deriving an indicator that is sensitive enough and 2) deriving a method that finds substand level damage areas. This study tackles the first problem.

Since observed forest damages [17] did not show marked change in the stand level mean backscattering of VH or VV polarization of S1 images, it is not probable that non-local mean backscattering coefficient values would improve the forest damage detection either. On the other hand, applying a window filter based on the standard deviations to the non-locally averaged backscattering would result in an image with a box pattern texture. In this study a non-local averaging method (STATSAR) is developed for retrieval of statistical parameters, such as mean, standard deviation, median, minimum, and maximum, in high resolution, such as 3 x 3 and 7 x 7 windows without the box pattern caused by speckle and the box-car filter.

STATSAR resembles the previously developed multitemporal non-local filtering method PIMSAR [13], but needs only one SAR image. In STATSAR 1) no assumptions about the scattering characteristics of the scenery are made in

The manuscript was submitted for review on November 26, 2021. This work was financially supported by Ministry of Agriculture and Forestry in the project Tuulituho-haukka.

T. Manninen is with the Finnish Meteorological Institute, FI-00101 Helsinki, Finland (e-mail: terhikki.manninen@fmi.fi).

E. Jääskeläinen is with the Finnish Meteorological Institute, FI-00101 Helsinki, Finland (e-mail: emmihenna.jaaskelainen@fmi.fi).

E. Tomppo is with the University of Helsinki, Department of Forest Sciences, Latokartanonkaari 7, P.O. Box 27, 00014 Helsinki, Finland. (e-mail: erkki.tomppo@helsinki.fi).

advance, 2) the non-local averaging is guided using only one dual polarization SAR image and 3) the similarity of pixels is sought using the 3 x 3 pixel window statistics. The method combines spatial statistics with k-means clustering to derive the guidance for the non-local averaging of diverse statistical parameters. In each cluster in the area of interest the pixels are averaged with the pixels that have the most similar 3 x 3 mean intensity.

II. Materials

This study is based on a set of S1 SAR Interferometric Wide (IW) Swath VV/VH images available in Ground Range Detected High (GRDH) resolution (10 m) format in the time range May – August, 2021 in Taivalkoski (65.6°N 28.8°E), northern Finland. Of special interest were the sub-swath IW2 images on the ascending pass just preceding (June 20) and succeeding (June 26) a major forest damage event on June 22, 2021. A digital elevation model of 2 m resolution (provided by National Land Surveying) was used for Doppler Range Terrain Correction of the SAR images.

The damage was exceptionally heavy in the region with a forest area of about four million hectares. From that, an area of about 40,000 - 50,000 hectares was so heavily damaged that re-planting was necessary, while a further 60,000 hectares would require sanitary cutting. In this study, a sub-area with a size of 19 km x 24 km was used for method development.

Five orthorectified airborne image of 0.5 m spatial resolution were available in 2018 and 2021 (after the forest damage) for comparison of the details of the filtered images [Fig. 1 and Fig. 2]. They were used to derive polygons containing/not containing forest damage in 2021 [Fig. 1]. Those polygons were used to calculate plot level backscattering statistics of damaged and not damaged forested areas. In addition, 248 circles each covering roughly 81 SAR pixels were drawn to sample areas of damage (124 circles) or no damage (124 circles) according to the airborne photos. The statistics of the VH backscattering of the circles were analyzed to study the effect of resolution on the possibility to distinguish forest damage. The circles covered only forest land with growing stock.

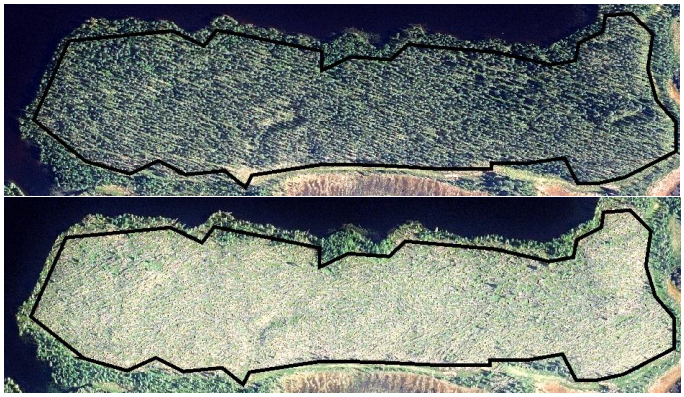

Fig. 1. An example of a complete forest damage of a plot from airborne photos of 2018 (top) and 2021 (bottom). National Land Survey of Finland Orthophoto Database 09/2021, Creative Commons Attribution 4.0 International License.

Fig. 2. An example of a subplot level limited forest damages from airborne photos of 2018 (top) and 2021 (bottom). National Land Survey of Finland Orthophoto Database 09/2021, Creative Commons Attribution 4.0 International License.

The damaged circles represented areas were almost all trees had fallen. As forest damage is not a binary feature, detecting a sufficient number of undamaged circles was challenging. Besides complete fall down the damage can appear as broken treetops and branches and half-outrooted trees leaning on each other. Those features are difficult to detect from the airborne images, hence the undamaged circles were preferably picked far from damaged areas. Yet, the representativity of the undamaged circles may be of lower quality than that of the damaged circles.

III. Method

The basis of STATSAR [Fig. 3] is the same as for the pixel based multitemporal non-local averaging method (PIMSAR) [13], namely k-means clustering [18][19][20][21] is used to divide the SAR image in 30 clusters of similar backscattering statistics within which the non-local mean is derived in the magnitude order of the average backscattering coefficient values. In PIMSAR the clustering was based on the multitemporal mean and standard deviation values of the backscattering coefficient of two polarizations, three swaths and two passes, whereas in STATSAR it is based on the mean, standard deviation, median, minimum, and maximum backscattering values derived in sliding 3 x 3 windows of VH and VV polarizations of a single S1 image. This window is called the base window and its size is chosen to be 3 x 3 pixels because the land cover is very heterogenous. In other kind of areas, a larger window size might produce more efficient speckle reduction without losing important small details.

The number of iterations of the k-means clustering was here 1000 and the number of individual samples (statistical parameter values) to be averaged non-locally is in this study 49, the same as when using PIMSAR. The construction of the guidance matrix used for deriving the non-local mean values of each cluster is explained explicitly in [13]. In STATSAR the

same kind of guidance matrix [Fig. 3] is used, but the criterion of the pixel ordering in each cluster is here the base window mean backscattering value (of the same polarization as the parameter to be filtered) instead of the multitemporal pixelwise mean used in PIMSAR.

The statistical parameters to be non-locally filtered, such as standard deviation or median, are calculated in a sliding box-car window of chosen size called the statistic window size. The non-locally filtered standard deviation of a certain window size is not identical to the standard deviation of the non-locally filtered backscattering coefficient of the same window size, as the latter alternative has an obvious box pattern, but their linear correlation is high. The coefficient of determination was for 3 x 3 window $R^2 = 0.74$ for the image of June 20, 2021.

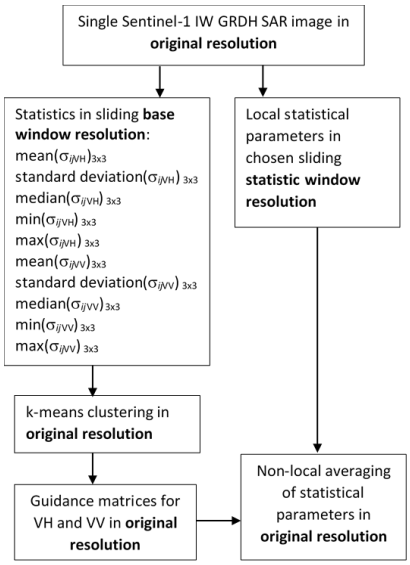

Fig. 3. The processing steps of the STATSAR method of averaging statistical parameters non-locally.

It should be noticed that although the STATSAR method is all the time based on the base window spatial statistics, the statistical parameters to be filtered can be calculated in a freely chosen window. As the standard deviation of natural targets typically depends on the window size, the STATSAR method can then provide every pixel with a wide variety of statistical features of varying spatial scales.

IV. Results

An example of a non-locally filtered standard deviation *s* representing a sliding 7 x 7 statistic window is compared to the standard deviation derived directly from the original image using the same sliding 7 x 7 window size in Fig. 4. The box pattern of the original standard deviation image does not appear in the non-locally filtered image. The same effect is seen in the images of the non-locally filtered mean, median, minimum, and standard deviation images: box pattern for box-car and no box pattern for non-locally filtered images.

The plot level standard deviation values of the original VH polarized images, denoted as $s(\sigma^0_{VH})$, before and after the storm are compared in Fig. 5. The size of the damaged plots varied in the range 1014 – 11614 pixels and the size of the undamaged

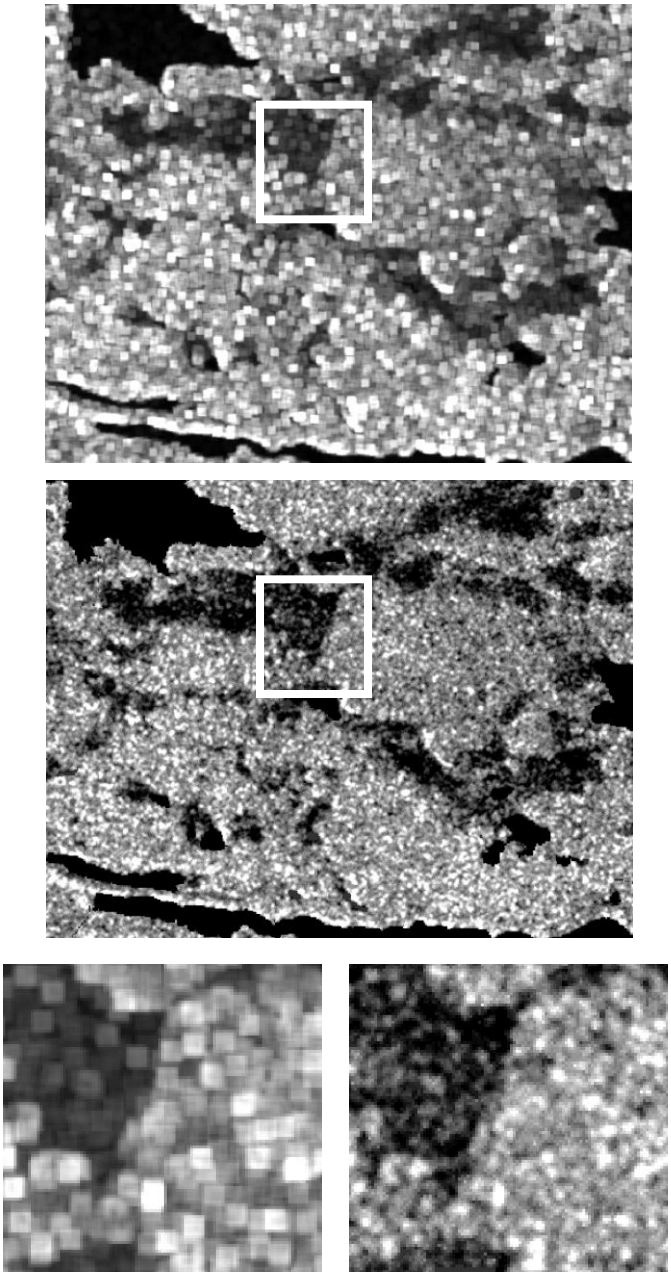

Fig. 4. The sliding 7 x 7 window standard deviation of the original VH polarized SAR image (top) of June 20, 2021, and the non-locally filtered 7 x 7 statistic window standard deviation (middle) of the same VH image. The area is an extract of the whole analyzed area and covers an area of about 21.5 km x 24.5 km. Open water is masked black. Extracts of the original image (bottom left) and the non-locally filtered image (bottom right) texture marked with white rectangles cover an area of about 1 km x 1 km.

plots varied in the range 1055 – 14883 pixels. The undamaged plots contained a mixture of forests and bogs. The corresponding comparison of the plot level averages of the non-locally filtered (denoted by <>) standard deviation values of 7 x 7 statistic window, denoted as $<s_{7x7}(\sigma^0_{VH})>$, is shown in Fig. 6. Both alternatives show that the variation of the backscattering is reduced by the damage. This is related to the reduced 3D structure of fallen trees. Indeed, in the plots, where the standard deviation is closer to that of undamaged plots, there are still a fraction of trees that have not fallen. As the size of the

plots is so large, the original images produce almost as clear distinction between damaged and undamaged plots as the non-locally filtered standard deviation.

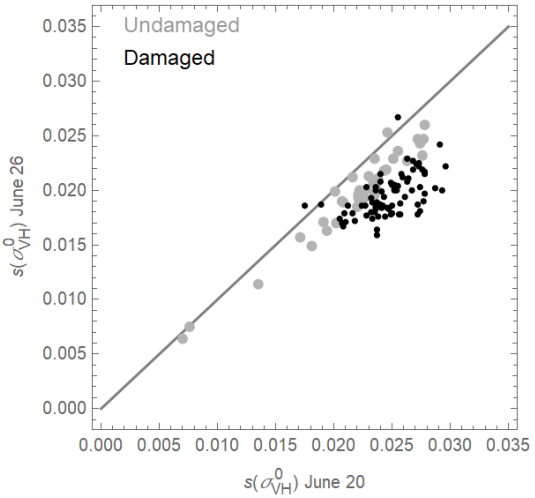

Fig. 5. The standard deviation of all VH polarized backscattering values within damaged and undamaged plot polygons in Taivalkoski before (June 20) and after (June 26) the storm.

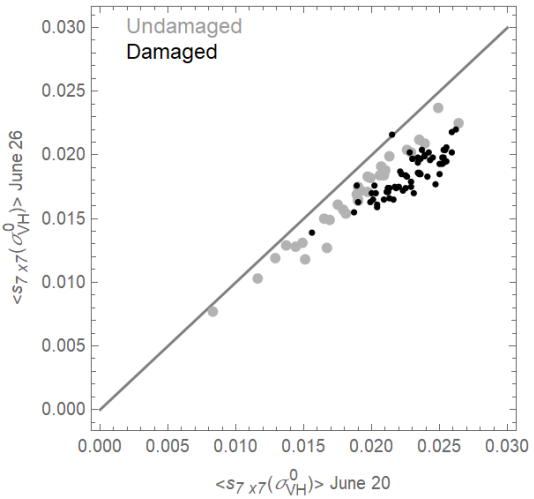

Fig. 6. The mean of the plot polygon texture of damaged and undamaged plots in Taivalkoski before (June 20) and after (June 26) the storm. The texture is described using the non-locally filtered 7 x 7 statistic window standard deviation of the VH polarized backscattering.

The effect of reducing the spatial averaging becomes obvious from the distributions. For the circles of 81 pixels, it is no more possible to use the standard deviation of the original VH polarized image backscattering coefficient to discriminate damaged plots from undamaged ones [Fig. 7], although also their backscattering characteristics are changed due to moisture conditions. However, for the circle average of the non-locally filtered 7 x 7 statistic window standard deviation the damaged and undamaged areas can still be distinguished. A nearest neighbor machine learning method [22][23] was employed to binary damage/no damage classification of the original circle level standard deviation $s(\sigma^0_{VH})$ and circle level mean of the non-locally filtered standard deviation of 3 x 3 and 7 x 7 statistical windows, $< s_{3x3}(\sigma^0_{VH})>$ and $< s_{7x7}(\sigma^0_{VH})>$, respectively. The circles were divided in the independent training and validation data sets by random picking. The confusion matrices are shown for the independent half of the data points not used for deriving the classification method [TABLE I — TABLE III]. Also, the combination of $< s_{3x3}(\sigma^0_{VH})>$ and $< s_{7x7}(\sigma^0_{VH})>$ was tested [TABLE IV]. The quality of the classification can be described with the critical success index *CSI*, which is calculated from the true positive (*TP*), false positive (*FP*) and false negative (*FN*) classification numbers

$$CSI = \frac{TP}{TP+FP+FN} \quad . \qquad (1)$$

In this context *TP* refers to damaged circles classified as damaged, *FP* refers to undamaged circles classified as damaged and *FN* to damaged circles classified as undamaged. The undamaged circles classified as undamaged represent the true negative cases (*TN*). The *CSI* values were 0.45, 0.57, 0.61 and 0.66 for $s(\sigma^0_{VH})$, $< s_{3x3}(\sigma^0_{VH})>$, $< s_{7x7}(\sigma^0_{VH})>$ and ($< s_{3x3}(\sigma^0_{VH})>$ & $< s_{7x7}(\sigma^0_{VH})>$), respectively. The reason for *FP* being higher than *FN* may result from the undamaged samples being in reality partly damaged. As after damage taken airborne photos existed only in a limited area, some of the undamaged circles were picked rather close to the major damaged zone in order to get a statistically meaningful data set. Unfortunately, from the airborne image it is possible to detect only the trunk level damage, not broken branches and twigs, which the radar detects. However, using the non-local filtering of the standard deviation enables analysis in higher resolution than when using the standard deviation derived from the original image. It also provides the possibility to benefit from variation of the backscattering in diverse scales, i.e., statistic window sizes.

The results demonstrated in this limited study are derived without paying attention to the effect of incidence angle variation (global or local) on the radiometry in the study region. When developing an operational method for forest damage detection, naturally those aspects have to be taken into account.

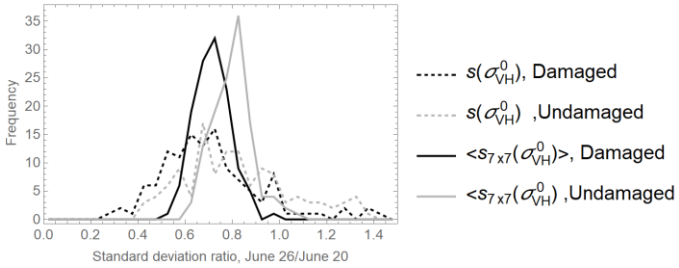

Fig. 7. The distributions of the ratio of standard deviation of the damaged and undamaged 81 pixel circles ($s(\sigma^0_{VH})$) after and before the storm are shown as dotted lines. The distributions of the mean of the non-locally filtered texture of the circles, as represented by $<s_{7x7}(\sigma^0_{VH})>$, are shown as solid lines.

V. Discussion and Conclusions

A new method to derive non-locally averaged statistical parameters STATSAR is presented for single dual polarization SAR images. The end result can be presented in original resolution, but it is recommended to be averaged in the base

TABLE I
CONFUSION MATRIX FOR CLASSIFICATION BASED ON $S(\sigma^0_{VH})$

Total 124	Classified damage	Classified no damage
Damage	*TP* = 42	*FN* = 20
No damage	*FP* = 31	*TN* = 31

TABLE II
CONFUSION MATRIX FOR CLASSIFICATION BASED ON $< S_{3x3}(\sigma^0_{VH})>$

Total 124	Classified damage	Classified no damage
Damage	*TP* = 48	*FN* = 14
No damage	*FP* = 22	*TN* = 40

TABLE III
CONFUSION MATRIX FOR CLASSIFICATION BASED ON $< S_{7x7}(\sigma^0_{VH})>$

Total 124	Classified damage	Classified no damage
Damage	*TP* = 50	*FN* = 12
No damage	*FP* = 20	*TN* = 42

TABLE IV
CONFUSION MATRIX FOR CLASSIFICATION BASED ON BOTH $< S_{3x3}(\sigma^0_{VH})>$ AND $< S_{7x7}(\sigma^0_{VH})>$

Total 124	Classified damage	Classified no damage
Damage	*TP* = 53	*FN* = 9
No damage	*FP* = 18	*TN* = 44

window, here 3 x 3 pixels, when using it for pixel basis operations. Statistical analyses should be carried out in sliding windows using the original resolution. The method offers a possibility to provide each pixel with a large versatility of statistical descriptors in several statistic window sizes without dominating speckle. STATSAR preserves the filtered image mean value.

When the change information is not required urgently, the previously developed multi-temporal PIMSAR method [13] should be applied similarly as STATSAR to filter the statistical parameters of interest, not only the intensity, into pixel resolution. PIMSAR based on single pixels of 6 images of the same swath and pass reduced speckle more efficiently than STATSAR based on 3x3 statistics: The mean, median and standard deviation values for the relative difference ((STATSAR – PIMSAR)/PIMSAR) of the non-locally filtered VH intensity of June 20 in original resolution were 0.005, -0.04 and 0.34, respectively.

The possibility to filter statistical parameters rather than the original intensity is useful in applications, where the texture of the image, not the intensity, reveals the changes. Naturally, both the intensity and texture changes can be taken into account using STATSAR.

REFERENCES

[1] Y. Zheng, X. Zhang, B. Hou, and G. Liu, "Using Combined Difference Image and k-Means Clustering for SAR Image Change Detection", IEEE Geoscience and Remote Sensing Letters, vol. 11, no. 3, pp. 691-695, 2014.

[2] F. Argenti, A. Lapini, L. Alparone, and T. Bianchi, "A tutorial on speckle reduction in synthetic aperture radar images," *IEEE Geosci. Remote Sens. Mag.*, vol. 1, no. 3, pp. 6–35, Apr. 2013.

[3] C.-A Deledalle, L. Denis and F. Tupin, "Iterative Weighted Maximum Likelihood Denoising with Probabilistic Patch-Based Weights", *IEEE Trans. Image Processing*, vol. 18, no.12, pp. 1-12, 2009.

[4] C.-A. Deledalle, L. Denis, G. Poggi, F. Tupin and L.Verdoliva, "Exploiting patch similarity for SAR image processing: The nonlocal paradigm", *IEEE Signal Process. Mag.*, vol. 31, no. 4, pp. 69–78, 2014.

[5] D. Gragnaniello, G. Poggi, G. Scarpa, L. and Verdoliva, "SAR Image Despeckling by Soft Classification", *IEEE J. of Selected Topics in Appl. EO and Remote Sens.*, vol. 9, no. 6, pp. 2118-2130, 2016.

[6] P.A.A. Penna and N.D.A. Mascarenhas, "(Non-) homomorphic approaches to denoise intensity SAR images with non-local means and stochastic distances", *Computers and Geosciences*, vol. 111, pp. 127–138, 2018.

[7] S. Vitale, D. Cozzolino, G. Scarpa, L. Verdoliva and G. Poggi, "Guided Patchwise Nonlocal SAR Despeckling", *IEEE Trans. Geosci. Remote Sensing*, vol. 57, no.9, pp. 6484-6498, 2019.

[8] G. Di Martino, A. Di Simone, A. Iodice, and D. Riccio, "Scattering-based non-local means SAR despeckling". *IEEE Transactions on Geoscience and Remote Sensing*, vol. 54, no. 6, pp. 3574–3588, 2016.

[9] R. Wang, N. He, Y. Wang, and K. Lu, "Adaptively weighted nonlocal means and TV minimization for speckle reduction in SAR images", *Multimedia Tools and Applications*, vol. 79, pp. 7633–7647, 2020.

[10] X. Su, C.A. Deledalle, F. Tupin, and H. Sun, "Two-step multitemporal nonlocal means for synthetic apertureradar images,"*IEEE Transactions on Geoscience and Remote Sensing*, vol. 52, no. 10, pp. 6181–6196, 2014.

[11] G. Chierchia, M. El Gheche, G. Scarpa, and L. Verdoliva,"Multitemporal SAR image despeckling based on block-matching and collaborative filtering,"IEEE Transactionson Geoscience and Remote Sensing, vol. 55, no. 10, pp.5467–5480, 2017.

[12] W. Zhao, C.-A. Deledalle, L. Denis, H. Maître, J.-M. Nicolas and F. Tupin, "Ratio-Based Multitemporal SAR Images Denoising: RABASAR", *IEEE Transactions on Geoscience and Remote Sensing*, Institute of Electrical and Electronics Engineers, 2019, 10.1109/TGRS.2018.2885683, hal-01791355v2.

[13] T. Manninen and E. Jääskeläinen, "Pixel Based Multitemporal Sentinel-1 SAR Despeckling PIMSAR," in IEEE Geoscience and Remote Sensing Letters, doi: 10.1109/LGRS.2021.3065300.

[14] E. Kalinicheva, D. Ienco, J. Sublime and M.Trocan, "Unsupervised Change Detection Analysis in Satellite Image Time Series using Deep Learning Combined with Graph-Based Approaches, *IEEE Journal of Selected Topics in Applied Earth Observations and Remote Sensing*, vol. 13, pp.1450-1466, 2020. 10.1109/JSTARS.2020.2982631

[15] X. Cao, Y, Ji L. Wang, B. Ji, L. Jiao, and J. Han, "SAR image change detection based on deep denoising and CNN", *IET Image Processing*, vol. 13, no. 9, pp. 1509-1515, 2019. https://doi.org/10.1049/iet-ipr.2018.5172

[16] E. Tomppo O. Antropov,J. Praks, "Boreal Forest Snow Damage Mapping Using Multi-Temporal Sentinel-1 Data", Remote Sensing., vol. 11, no. 4, pp. 384, 2019. https://doi.org/10.3390/rs11040384

[17] E. Tomppo, G. Ronoud, O. Antropov, H. Hytönen, J. Praks,, "Detection of Forest Windstorm Damages with Multitemporal SAR Data—A Case Study: Finland", Remote Sens., vol. 13, pp. 383, 2021. https://doi.org/10.3390/rs13030383

[18] J. MacQueen, "Some methods for classification and analysis of multivariate observations", Proceedings of the Fifth Berkeley Symposium on Mathematical Statistics and Probability, Volume 1: Statistics, pp. 281-297, University of California Press, Berkeley, Calif., 1967. https://projecteuclid.org/euclid.bsmsp/1200512992.

[19] J.A. Hartigan and M.A. Wong, "A K-Means Clustering Algorithm", *Journal of the Royal Statistical Society: Series C (Applied Statistics)*, vol. 28, pp. 100-108, 1979. https://doi.org/10.2307/2346830

[20] S.P. Lloyd, "Least squares quantization in PCM", *IEEE Trans. Inf. Theory*, vol. 28, pp. 129-136, 1982.

[21] E. Tomppo and M. Halme, "Using coarse scale forest variables as ancillary information and weighting of variables in k-NN estimation: A genetic algorithm approach." Remote Sensing of Environment, vol. 92, no. 1, pp. 1–20, 2004.. doi:10.1016/j.rse.2004.04.003.

[22] Fix, E., & Hodges, J. L. (1989). Discriminatory Analysis. Nonparametric Discrimination: Consistency Properties. International Statistical Review / Revue Internationale de Statistique, 57(3), 238–247. https://doi.org/10.2307/1403797

[23] Altman, N. S. (1992). An Introduction to Kernel and Nearest-Neighbor Nonparametric Regression. The American Statistician, 46(3), 175–185. https://doi.org/10.2307/2685209